On the use of Acoustic Wind Tunnel Data for the Simulation of sUAS Flyover Noise

Stephen A. Rizzi[1], Nikolas S. Zawodny[2] and Nicole A. Pettingill[3]
NASA Langley Research Center, Hampton, VA 23681, USA

Acoustic measurements of a small, unmanned aerial system were recently acquired during a ground test campaign. The purposes of the ground test, conducted in the NASA Langley Low Speed Aeroacoustic Wind Tunnel, were to characterize the source noise in terms of its tonal and broadband content, and to identify conditions under which multirotor and rotor-airframe interactions are present. The focus of this work is to assess the effectiveness of using those data for the simulation of flyover noise at a ground observer. The assessment is made at two levels of fidelity using different sets of tools. In the first, 1/3 octave band spectra at a ground receiver will be simulated in a frequency domain approach using the NASA Aircraft NOise Prediction Program. In the second, the pressure time history at a ground receiver is simulated in a time domain approach using the NASA Auralization Framework. Various objective measures are used to verify the simulation process. Acoustic wind tunnel and flight test data are used to gain insight into perceptually important effects.

Nomenclature

c_o	=	speed of sound (m/s)
f	=	frequency (Hz)
M	=	Mach number
r	=	slant range (m)
R	=	rotor blade radius (m)
t	=	time (s)
ϕ	=	azimuthal directivity angle (deg.)
θ	=	polar directivity angle (deg.)

I. Introduction

SMALL, unmanned aerial systems (sUAS) are being promoted for a number of different uses including package delivery, inspection, and surveillance. If such operations become ubiquitous, then their noise impact must be assessed, particularly in urban settings, in which the density of aircraft may be high, and in which operations are in proximity to humans. Data for such assessments may come from flyover measurements of actual sUAS. However, such data are not generally available for vehicles under development. Therefore, there is an incentive to utilize ground test data that may be acquired for some other purpose, e.g., source noise characterization and/or noise reduction technology development, as the basis of noise impact assessments. The purpose of this paper is to consider two approaches for doing so, using ground and flight test data to determine the effectiveness of each approach.

Both approaches utilize the same acoustic data set as a starting point. In this work, the data were acquired from a small quadcopter [1] tested in the NASA Langley Low Speed Aeroacoustic Wind Tunnel (LSAWT) [2]. The processed wind tunnel data consist of sets of synchronously averaged time domain data representing the periodic tonal components, and uncorrelated narrowband spectra ideally representing all sources of residual broadband noise. In the first approach, the wind tunnel data are condensed to a set of 1/3 octave band spectra at the source, and propagated with a frequency domain approach using the NASA Aircraft NOise Prediction Program (ANOPP) [3]. The result is a time history of 1/3 octave band spectra at a ground receiver. In the second approach, the periodic and broadband pressure time histories are synthesized at the source and propagated in a time domain approach using the NASA Auralization Framework (NAF) [4]. The combined process of synthesis and propagation is referred to as auralization [5], and results in a pressure time history at a ground receiver, referred to as a pseudorecording. Both sets of results may be further processed into various noise metrics for comparison with those derived from the wind tunnel and

[1] Senior Researcher for Aeroacoustics, Aeroacoustics Branch, AIAA Fellow
[2] Research Aerospace Engineer, Aeroacoustics Branch, AIAA Member
[3] Research Aerospace Engineer, Aeroacoustics Branch, AIAA Member

flyover recordings [6]. However, the time domain approach offers the advantage that the resulting pseudorecording can be used for psychoacoustic metrics calculations and as test stimuli in psychoacoustic studies.

The paper first summarizes the wind tunnel measurements and details the associated data processing. The two simulation methods are then presented, with emphasis on the time domain approach. Comparisons with wind tunnel data are used to verify the simulation processes. A brief summary of the flight test measurements is made and comparisons of the simulations with flight test data are used to gain further insight into perceptually important features.

II. Acoustic Wind Tunnel Measurements

All data used in this work were collected from a Straight Up Imaging (SUI) Endurance, a 3.2 kg empty weight quadcopter used for imaging/surveying purposes. Images of the vehicle mounted on the LSAWT model test stand (MTS), as well as the rotor directions of rotation, are provided in Figure 1. Each rotor consists of two carbon fiber fixed-pitch blades, each with a blade radius of R = 190.5 mm (7.5 in).

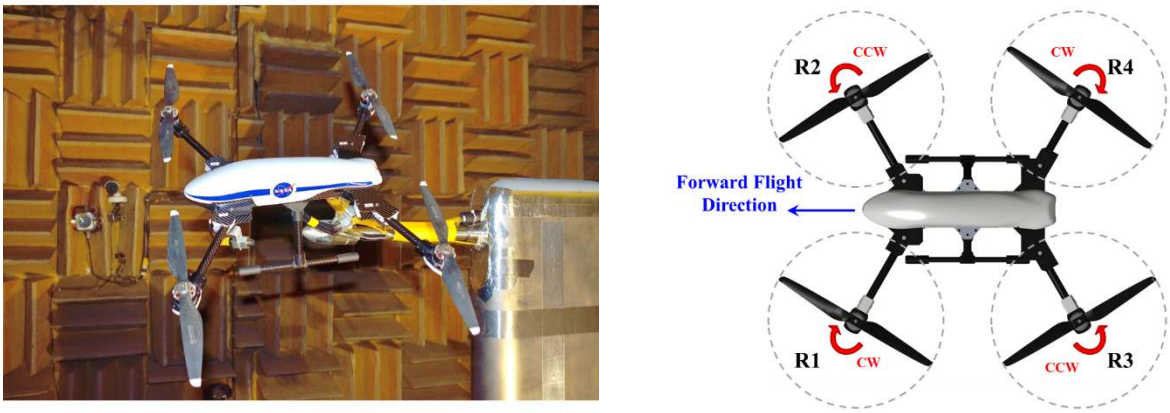

(a) Image of vehicle installed on MTS. (b) Rotor nomenclature (top view).

Figure 1: The SUI Endurance quadcopter.

The acoustic testing configurations are summarized in Figure 2. A total of four azimuthal microphone survey orientations were tested by rotating the vehicle airframe on the MTS relative to the LSAWT linear microphone array, see Figure 2(a). A fixed lateral separation distance of 3.54 m (~18.5R) was maintained between the microphone elements and the center of the vehicle. The polar extents of the microphones are shown pictorially in Figure 2(b). While this image presents the microphone array in the flyover configuration, the indicated range of microphone polar angles is applicable to all measured azimuthal orientations indicated in Figure 2(a). Additional details of the wind tunnel test campaign may be found in Ref. [1].

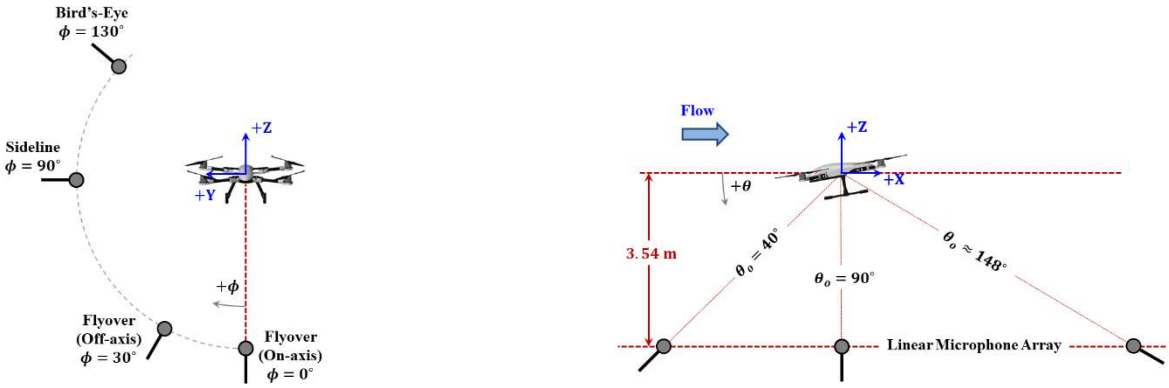

(a) Azimuthal (ϕ) angles of array surveys. (b) Polar (θ) angles of flyover microphones.

Figure 2: Linear microphone array survey orientations: (a) upstream view of azimuthal plane (flow is into page), (b) profile view of polar plane (flyover configuration). Note images not drawn to scale.

A. Data Processing

Time series pressure data were simultaneously sampled at 80 kHz for 12 seconds across the 28-element linear microphone array, as described in Ref. [1]. Data processing, beyond calibration to engineering units, was required to not only gain insight into the relative contributions of periodic and broadband components [1], but also to generate the source noise definitions required of the frequency and time domain simulation approaches [7]. The subsequent data processing steps are depicted in Figure 3. Following calibration of microphone data to engineering units, the signal is separated into periodic and broadband components in the time domain, according to method 2 in Ref. [1]. Briefly, that process uses the average tachometer signal for each rotor to extract once-per-revolution data followed by a synchronous time-average. The periodic component is obtained by replicating the synchronous time-average data over the number of required revolutions, while the broadband component is obtained by subtracting that from the original signal. For single rotor data, the process results in one periodic and one broadband component. For simultaneous operation of two rotors, the process is applied twice, and results in two periodic components and two residual components. At each frequency, the minimum narrowband spectral density (PSD) between the two residual components results in a single combined broadband component (expressed in narrowband PSD form) for the simultaneously running rotor pair. The process was not applied to measurements taken on the full vehicle (simultaneous operation of four rotors) because the forward pair (rotors R1 and R2) and aft pair (rotors R3 and R4) operate at nearly the same revolutions per minute (RPM). Therefore, subsequent simulation of the full vehicle noise is based on the two rotor operations. The PSD of the tunnel tare reading is subtracted from the PSD of the broadband component, and the difference is converted to the narrowband sound pressure level (SPL) of the broadband component. A similar operation takes place on the total (unseparated) signal for use in the ANOPP frequency domain approach.

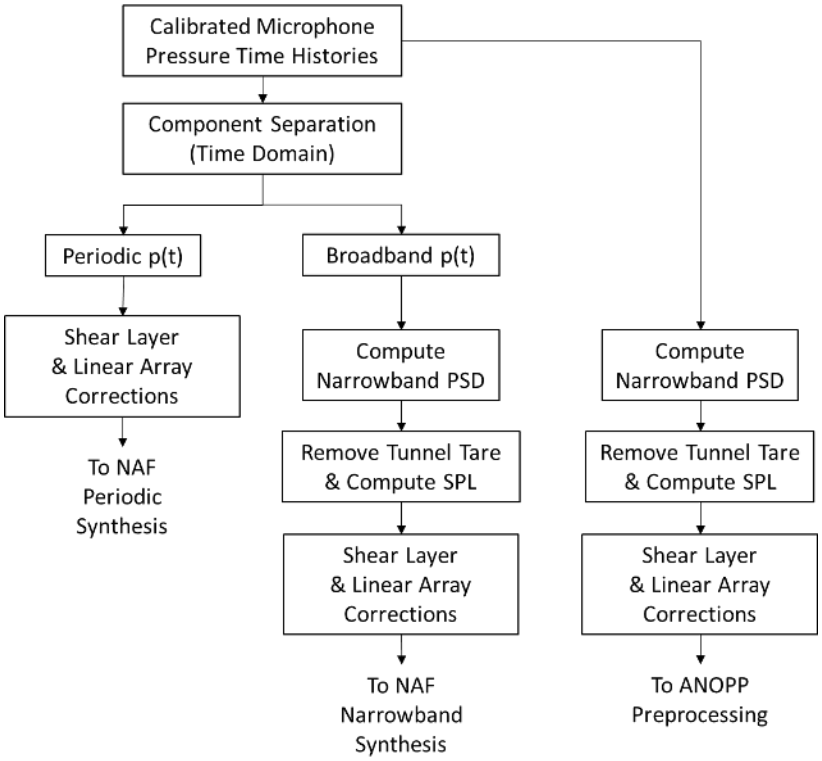

Figure 3: Flowchart of microphone data processing.

The data were amplitude-corrected for both shear layer and microphone array effects. A cylindrical shear layer correction was applied to account for potential refraction of sound waves through the open-jet shear layer [8]. This resulted in an amplitude correction, L_{SL}, and a physical microphone location correction in terms of the source-to-microphone distance (slant range) and polar angle, r_{SL} and θ_{SL}, respectively. Due to the low freestream velocity associated with these cases, the shear layer amplitude corrections were very small for all microphones (within ± 0.5 dB). A second amplitude correction was applied to normalize the linear array data to a common radial reference distance (r_{ref} = 3.54 m), that is, the geometrical distance associated with the closest microphone. Those corrections

were much greater, ranging from 0^+ dB at the nearest microphone (not identically 0 due to the shear layer correction) to +5.7 dB at the most downstream microphone. To summarize, the amplitude correction in dB, and angle correction in degrees are given by

$$L_{Corr} = L_{SL} + 20\log_{10}\left(r_{SL}/r_{ref}\right) \tag{1}$$

and

$$\theta_{Corr} = \theta_{SL} - \theta_o \leq 3.2° \tag{2}$$

in which θ_o represents the geometric polar directivity angle.

In addition to the amplitude correction, the periodic component was phase aligned to account for the time delay associated with i) the change in path length between the linear array and the common radial reference distance, and ii) convective effects. This alignment is needed to minimize artifacts in the subsequent periodic synthesis [9]. The time delay is given by

$$t_d = \frac{r_{SL} - r_{ref}}{c_o\left(1 + \dfrac{M_\infty}{\cos\theta_{SL}}\right)} \tag{3}$$

in which c_o is the speed of sound and M_∞ is the freestream Mach number at the tunnel operating condition. The time delay is compensated to the nearest sample, which was judged to be sufficient at the sampling rate of 80 kHz. Application of the time delay to the broadband data is not required because the phase is random.

The combined effects of the amplitude correction and phase alignment on the periodic data are shown in Figure 4 for the 28 microphones in the linear array. The data shown are for one revolution, or two blade passages. In Figure 4(a), the lack of amplitude and phase correction are evident in the variance between traces, whereas the amplitude and phase-corrected traces in Figure 4(b) are seen to collapse upon each other, with remaining differences largely attributable to differences in source directivity.

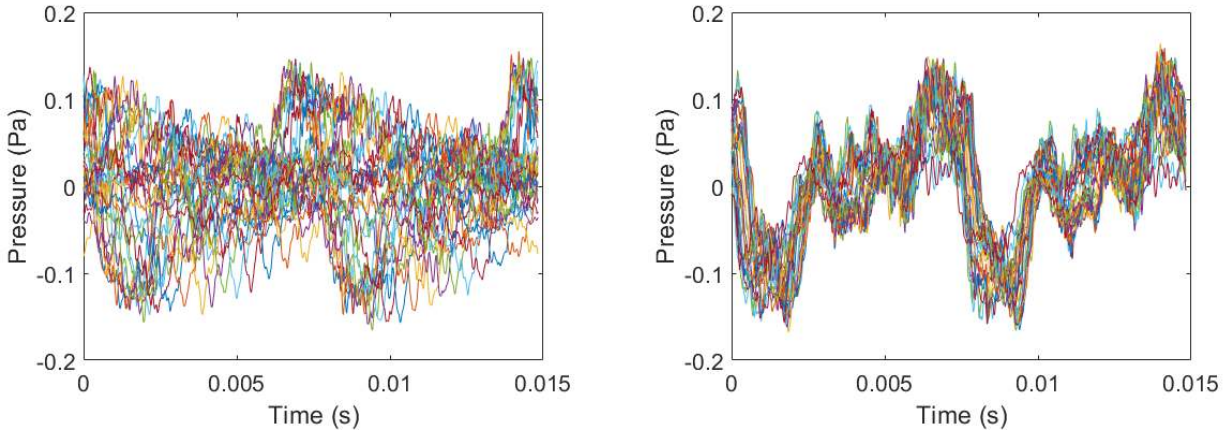

(a) Uncorrected. (b) Amplitude and phase corrected.

Figure 4: Periodic time histories of 28 microphones for individual rotor (R1) operation at 45 N net thrust condition.

Finally, the amplitude-corrected total SPL serves as input to the ANOPP analysis, as described in Section III.A. One revolution of the amplitude and phase-corrected periodic data, and the amplitude-corrected broadband SPL serve as input to the NAF periodic and narrowband syntheses, respectively, as described in Section III.B.

The data set associated with the simultaneous operation of rotors R1 & R3 is used for subsequent flyover simulations. An example of the SPL data for the geometric polar directivity angle θ_o = 70° is shown in Figure 5 on a (a) narrowband and (b) 1/3 octave band basis. In Figure 5(b), it is seen that the transition from tonal-dominated to broadband-dominated noise occurs at a 1/3 octave band center frequency of 1.25 kHz. Figure 5(b) also shows the summation of individually operated rotors R1 + R3, in which this transition occurs at about 2.5 kHz and at a lower amplitude than the simultaneous case. The difference is indicative of multirotor interactions that must be taken into account in any subsequent modeling effort.

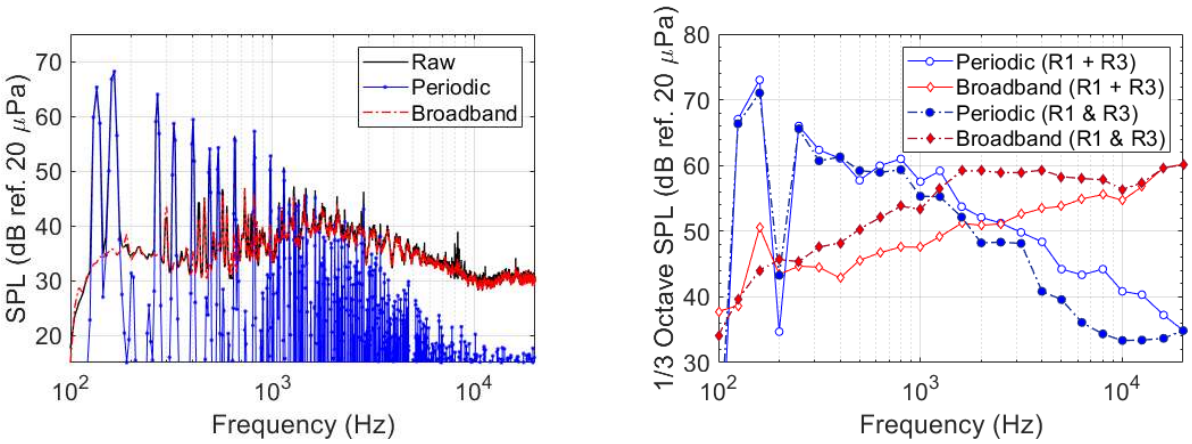

(a) R1&R3 narrowband spectra.

(b) R1+R3 and R1&R3 1/3 octave band spectra.

Figure 5: Separated periodic and broadband spectra for simultaneous rotor operation (R1&R3) and summed individual rotor operation (R1+R3) for the 45 N net thrust condition, on-axis flyover orientation at θ_o = 70°.

III. Flyover Simulation Methods

Two different approaches are used to simulate flyover data at the flight test microphone positions. One approach is performed in the frequency domain and the other in the time domain. Both have previously been shown to provide comparable certification type noise metrics when the operations start from the same data, e.g., see Ref. [5].

A. Frequency Domain Approach

While the ANOPP [3] has several semiempirical source models for generating source noise data, the ANOPP ACoustic Data (ACD) module is used in this work. The ACD module allows user-provided source data to be specified. The data are derived from the amplitude-corrected total SPL data (see Figure 3), following the additional ANOPP specific preprocessing steps next described. A flowchart depicting this process is shown in Figure 6. A similar approach was employed in Ref. [7].

The ACD module requires data in the same form as would be produced by the semiempirical source models in ANOPP, namely, as Doppler-shifted 1/3 octave band SPL. The amplitude-corrected total SPL data, expressed in narrowband form, are first interpolated to 1° emission angle increments. The data are not extrapolated beyond the range of shear layer-corrected emission angles. Thus, the amplitude-corrected total SPL data for microphone 1 are used for polar angles forward of microphone 1, and the amplitude-corrected total SPL data for microphone 28 are used for angles aft of microphone 28. Next, the frequency vector at each angle increment is Doppler-shifted according to

$$f_{Flight} = f_{Tunnel} / [1 - M_{Flight} \cos \theta_{SL}] . \tag{4}$$

In this manner, the data continue to be Doppler-shifted outside the range of measurements even though the underlying source spectra remain unchanged. Finally, the data at each angle increment are summed into 1/3 octave bands ranging from 50 Hz to 10 kHz.

The ANOPP is a time marching simulation program in which the frequency domain source data are propagated to one or more receiver positions. The path between the source and the receiver is evaluated at the reception time. Once the emission position is found, the emission angle along the straight-line path is calculated, and the source data are determined through interpolation of the 1/3 octave band SPL data. The interpolated 1/3 octave band SPL data are propagated to the ground observer location through application of spherical spreading loss, atmospheric absorption, and ground plane effects (if any). This operation is performed in the ANOPP-PRO module. Note that the propagation time delay is already taken into account when finding the emission position. The operation is repeatedly performed, typically at 0.5 second intervals, over the course of the flyover event. The result is a time history of 1/3 octave band SPL spectral data at the receiver position(s), that can be further processed within ANOPP to give unweighted and A-weighted SPL (L_A), A-weighted sound exposure level (L_{AE}), perceived noise level (PNL), tone-corrected perceived noise level (PNLT), and effective perceived noise level (EPNL).

B. Time Domain Approach

The NAF [4] also uses a time marching approach, and its operation is depicted in Figure 7. For each time step, the NAF Path Finder first determines the path between the source and receiver at emission time. The NAF time step is much finer than the ANOPP time step, typically on the order of 10 ms. The emission angle is calculated and passed to the NAF synthesis engine, where the source data are synthesized to produce a segment of pressure time history data (audio) for the current time increment. Audio data are represented by red lines in Figure 7. Within the NAF, a source describes a set of colocated components, e.g., the periodic and broadband components constitute the rotor noise source. All components within a source share a common path. An overview of NAF synthesis methods can be found in Ref. [5], and those specific to this effort are described in Sections III.B.1 and III.B.2. In parallel with the synthesis operation, the NAF Path Traverser determines the attenuation associated with spherical spreading, the delay associated with the propagation time, and spectral modification associated with the atmospheric absorption and ground effect (if any). These are cast as a series of gains, time delays, and filters (GTF) that operate on the synthesized audio signal to generate the pressure time history (pseudorecording) at the observer. The time rate of change of the time delay simulates Doppler shift. Therefore, the steps taken to Dopplerize the source data for the ANOPP ACD module are not required for the NAF. Optional post-processing of the resulting pseudorecording using the ANOPP2 Acoustics Analysis API [10] for certification type metrics, or the NAF Psychoacoustic Analysis Library (PAL) for sound quality metrics, is not depicted in Figure 7.

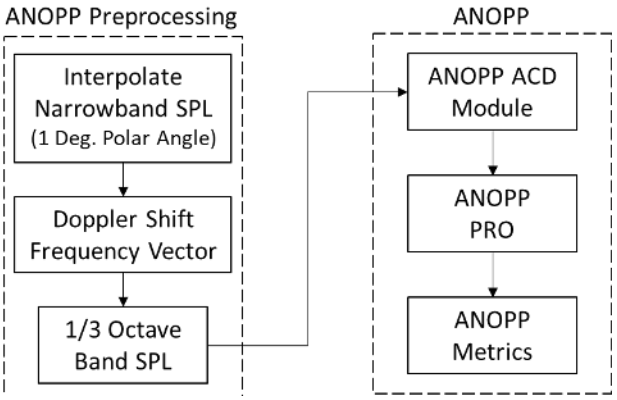

Figure 6: Frequency domain simulation approach using the ANOPP.

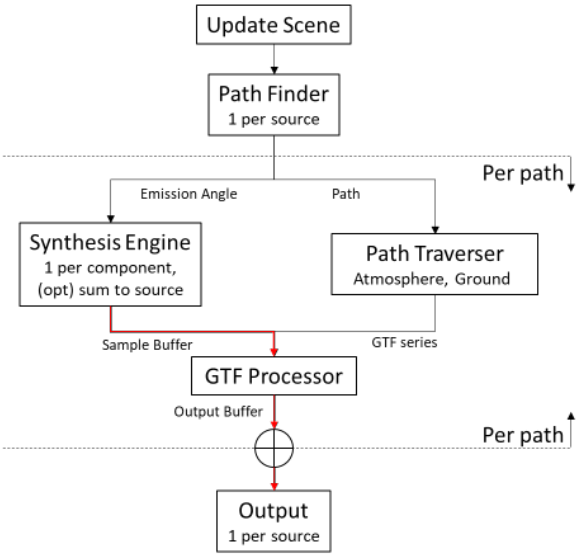

Figure 7: Time domain simulation approach using the NAF.

1. *Periodic Synthesis*

The periodic rotor noise is synthesized according to an additive synthesis method, following that described in Refs. [9, 11]. The set of periodic data, obtained by the process depicted in Figure 3, serves as input for a particular test condition. At each emission angle, the data are analyzed using a discrete Fourier transform over a period of one revolution, as depicted in Figure 4(b). The resulting amplitude and phase are thus specified at the shaft order frequencies, that is, at the blade passage frequency (BPF) divided by the number of blades per rotor (2 for the SUI Endurance). This differs from the usual approach taken when data are provided by a steady analysis. There, the pressure time history is periodic on the blade passage period, not on the period of revolution. From a practical perspective, this doubles the number of harmonics to synthesize, and hence doubles the computational effort.

The sound pressure is synthesized at the audio sampling rate (typically 44.1 kHz) according to

$$p(t,\theta,\phi) = \sum_{n=1}^{N} A_n(\theta,\phi)\cos\left[2\pi f_n t + \psi_{o,n}(\theta,\phi)\right] \tag{5}$$

in which f_n, A_n, and $\psi_{o,n}$ are the frequency, magnitude, and phase of the n^{th} shaft order harmonic. The decomposition and reconstruction essentially amount to a Fourier and inverse Fourier transform, and therefore, recreates the waveform, at the audio sampling rate. In a flyover simulation, the amplitude and phase are interpolated to the

instantaneous emission angles, sample by sample. The steps taken to align the phase, per equation (3), help to maintain the desired waveform, as observed in Ref. [9].

An example of the synthesis process is shown in Figure 8(a) for an individual rotor. Here it is seen that the average of the two blade passages (shown replicated in red), is a close facsimile of the once per revolution data from which it was computed (black). The narrowband SPLs, shown in Figure 8(b) and computed from 12 second records, however, indicate that the average data lack odd harmonics of the shaft order frequency (BPF/2 = 67 Hz). Visually, one might conclude that those frequencies are unimportant as they are 10s of dBs lower than the BPF peaks in most cases. On the basis of the overall SPL (OASPL), that would be true; 71.43 dB vs. 71.37 dB for the one per revolution and averaged BPF data, respectively. However, the more harmonically rich sound generated by inclusion of shaft order harmonics is clearly evident upon auditioning the sounds (audio samples 1-2, available for download [12]). Further, the data suggest that if the source noise description were to be provided by analysis and if the data were to be used in psychoacoustic studies, then additional steps should be taken to generate shaft order harmonics, e.g., modeling each blade geometry slightly different from the others, or accounting for unsteady inflow.

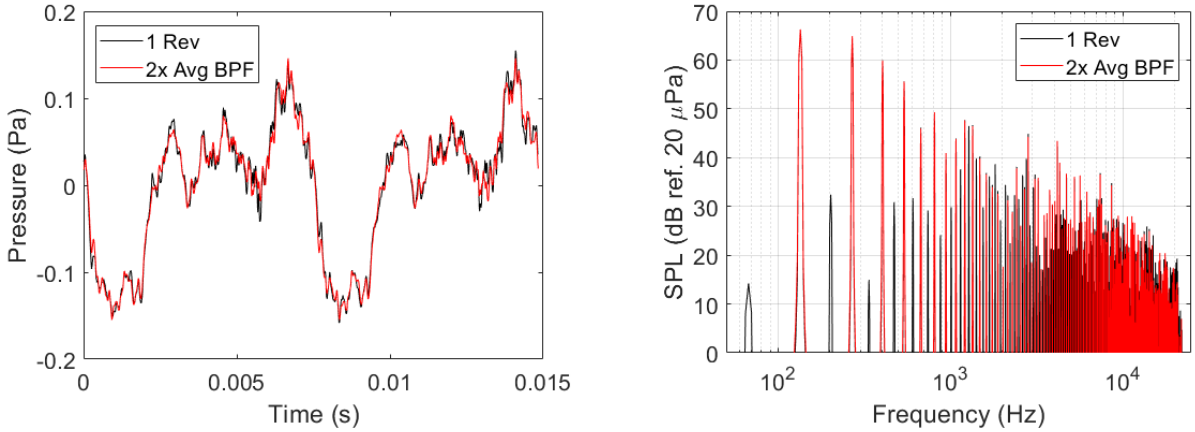

(a) Pressure time history. (b) Narrowband SPL.

Figure 8: Comparison of syntheses using one revolution and average BPF data from individual rotor (R1) operation at the 45 N net thrust condition, on-axis flyover orientation at θ_o = 70°.

2. Broadband Synthesis

The broadband noise is synthesized according to a subtractive method, in which the source noise description, provided as the corrected narrowband SPL data by the process depicted in Figure 3, serves as the basis for a filter that operates on a white noise input signal. More details on the general approach are provided in Ref. [5]. For this work, a new NAF plugin library was written to allow the source noise description to be provided in narrowband form, instead of the more typical 1/3 octave band form. Since the input data may be specified at a different frequency resolution than that associated with the block-by-block broadband synthesis in the NAF, the data are interpolated to the appropriate frequency resolution using a spline fit prior to synthesis. Broadband synthesis typically runs at a block size of 16,384 points at 44.1 kHz, giving a frequency resolution of 2.69 Hz. In the flyover simulation, the spectral amplitudes are first interpolated at the original sampling rate, according to the emission angle at the block time of emission, then interpolated to the frequency resolution needed for NAF synthesis.

A short segment of data from the broadband synthesis process is shown in Figure 9(a). Also shown is a segment of the separated, amplitude-corrected broadband pressure time history that was used for the source noise definition. The traces are offset for clarity. For the purposes of this set of comparisons, note that the LSAWT tunnel tare reading was not removed, as this operation can only be performed on the narrowband PSD, see Figure 3. While the two traces appear to differ in magnitude, that difference is small in terms of OASPL; 64.9 dB versus 64.2 dB for the tunnel and synthesized data, respectively. These differences are attributable to the resampling needed for synthesis at the audio sampling rate. Inspection of the resulting narrowband SPL, shown in Figure 9(b), shows the spectral differences to be small. The broad low frequency peak below 100 Hz is attributable to the tunnel tare, which would normally have been removed.

Referring back to the LSAWT pressure time history data in Figure 9(a), the periodicity of the peaks is at the BPF. A similar periodicity has been noted in helicopter data and was found to be attributable to convective amplification associated with the blade rotation [13]. The inflow condition of the rotating blades is another potential modulation source. The synthesized sound does not exhibit this behavior because it is based on the time-averaged narrowband

SPL data shown in Figure 9(b). The difference is striking when the sound is auditioned (audio samples 3-4 [12]), with the LSAWT data exhibiting a rough character and the synthesized data a smoother character.

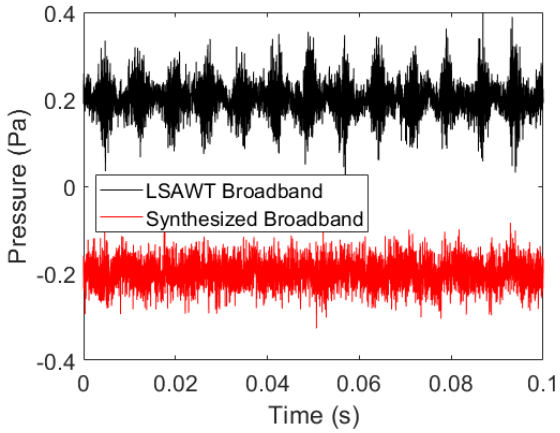

(a) Pressure time history.

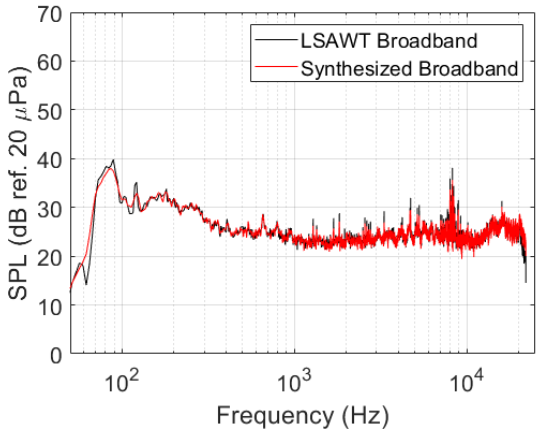

(b) Narrowband SPL.

Figure 9: Comparison of LSAWT and synthesized broadband data of individual rotor (R1) operation at the 45 N net thrust condition, on-axis flyover orientation at θ_o = 70°.

The presence of the amplitude modulation in the LSAWT data is evident in the Morlet wavelet energy spectrum shown in Figure 10(a), and its absence in the synthesized data in Figure 10(b). The spectra were computed by the method in Ref. [14]. This view indicates that the modulation mostly affects the higher frequencies.

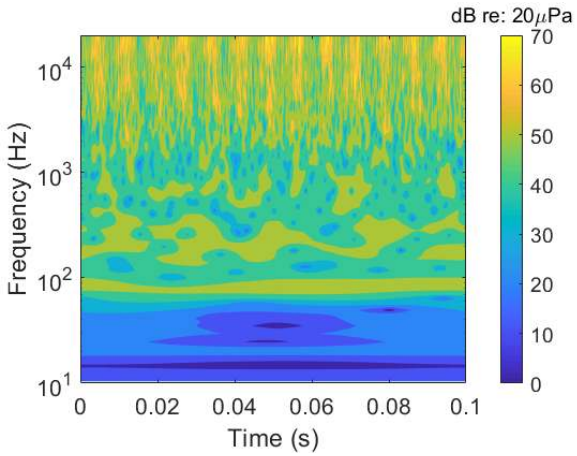

(a) LSAWT data.

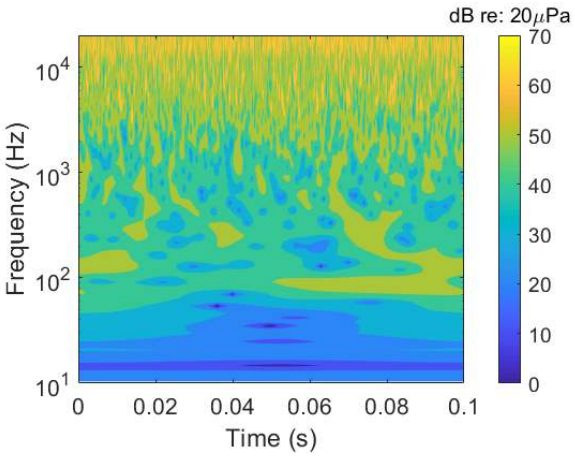

(b) Synthesized data.

Figure 10: Comparison of wavelet energy spectra of broadband noise of individual rotor (R1) operation at the 45 N net thrust condition, on-axis flyover orientation at θ_o = 70°.

In terms of sound quality, the effect of these modulation manifests itself as roughness [15], that is, the sound attribute that reflects the perception of rapid amplitude modulation, in the range of 15-300 Hz, with a maximum impression when the fluctuations are at about 70 Hz. The BPF of this data, 135 Hz, falls within that range. Sound quality metrics were computed using the NAF Psychoacoustic Analysis Library (PAL). There currently exists no standard for the calculation of roughness. The implementation used in this work was based on that of Daniel and Weber [16]. A comparison of time-varying roughness, calculated for 12 second records, is shown in Figure 11(a), where it is seen that the roughness of the LSAWT data greatly exceeds that of the synthesized data. Time-varying loudness, reflecting the human perception of the magnitude of the sound over time, was calculated by the standardized Zwicker method [17]. Sharpness, calculated using DIN 45692 [18], is an indicator of spectral balance of a signal. Given that the spectral amplitudes of the two data sets are nearly identical, it is not surprising that the loudness and sharpness shown in Figure 11(b) are similar between data sets. Finally, fluctuation strength (not shown), reflecting perception of slow fluctuations (1-16 Hz), is very low for both data sets.

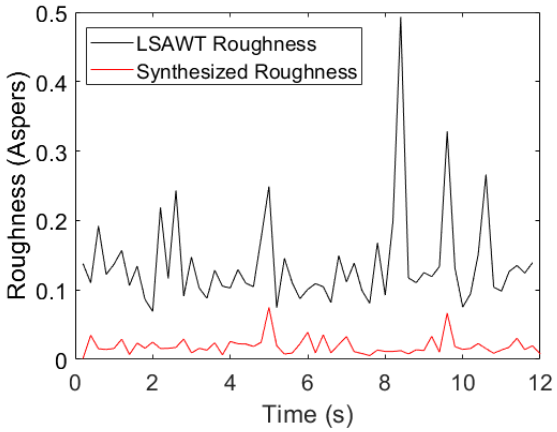

(a) Roughness.

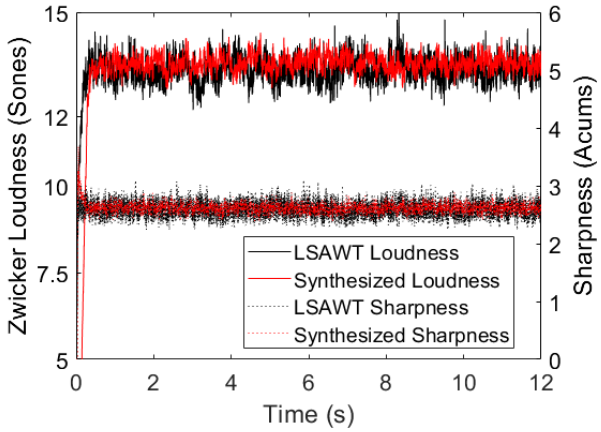

(b) Loudness and sharpness.

Figure 11: Comparison of sound quality metrics of broadband noise of individual rotor (R1) operation at the 45 N net thrust condition, on-axis flyover orientation at $\theta_o = 70°$.

3. Total Rotor Noise Source

The total rotor noise source is obtained by summing the synthesized periodic and broadband time history data. A comparison of the narrowband SPL of the synthesized and LSAWT total rotor noise data is shown in Figure 12(a). Excellent agreement is seen in terms of the spectral shape and in terms of OASPL, 72.2 dB in each case. The wavelet energy spectrum of the LSAWT total rotor noise data in Figure 12(b) indicates the presence of amplitude modulations at high frequencies, and reinforces the assertion that the modulations are not artifacts of the periodic/broadband separation process. Indeed, the same rough character can be heard in the auditioned sound of the LSAWT total noise, and not in the synthesized tonal noise (audio samples 5-6 [12]). The bright horizontal bands in Figure 12(b) are attributed to the BPF and 2BPF tones.

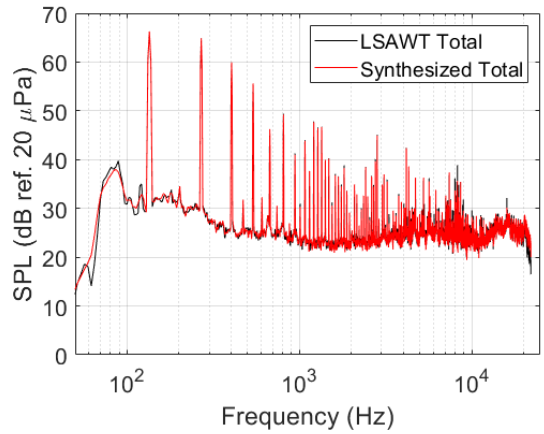

(a) Narrowband SPL.

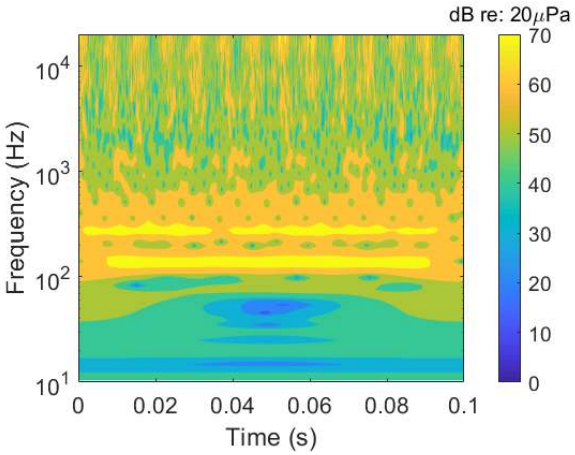

(b) Wavelet energy spectrum of LSAWT total.

Figure 12: Comparison of total noise of individual rotor (R1) operation at the 45 N net thrust condition, on-axis flyover orientation at $\theta_o = 70°$.

Similar observations can be made of the simultaneous rotor operation (R1&R3) data that serve as the basis for the flyover simulations. The narrowband SPL spectra compare favorably, see Figure 13(a), with the LSAWT and synthesized data having the same OASPL of 76.4 dB. In Figure 13(b), the modulations are less regular than the individual rotor operation, but the difference in the sound quality between the LSAWT and synthesized sound remains apparent upon auditioning (audio samples 7-8 [12]).

To summarize the time domain approach, there are two important observations. First, the inclusion of shaft order harmonics may have a significant effect on the perceived sound. Methods fortunately exist in the current tool set to generate those data for either experimental or numerical analyses. Second, the inclusion of high frequency broadband modulation is perceptually important. While it is clearly possible to incorporate those time varying effects in the

synthesis, current approaches for source definition, whether stemming from experimental or analytical/numerical analyses, are typically limited to providing time-averaged spectral data. Some additional effort will be required to generate data in the future that do not have this limitation. Neither of the two observations is applicable to the frequency domain approach (as cast above), as all such information is lost when summing the narrowband spectra into 1/3 octave bands.

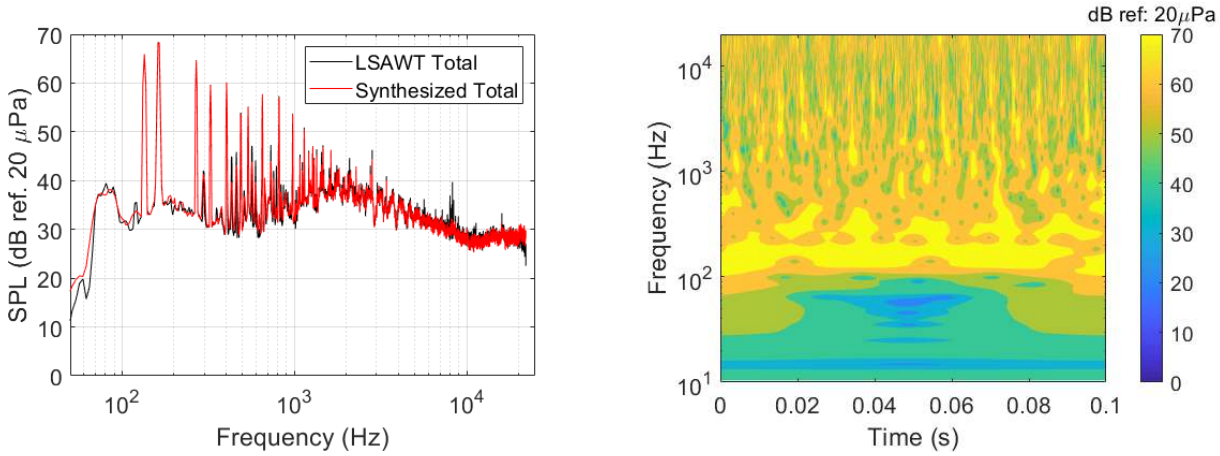

(a) Narrowband SPL. (b) Wavelet energy spectrum of LSAWT total.

Figure 13: Comparison of total noise of simultaneous rotor (R1&R3) operation at the 45 N net thrust condition, on-axis flyover orientation at $\theta_o = 70°$.

IV. Flight Test Measurements

A series of flight tests were performed in 2016 in the Cleveland National Forest about 35 miles NE of San Diego, CA. The Endurance performed autopiloted, straight and level flyovers at nominally 5 and 10 m/s speeds, and at 20, 30, 50, and 100 m above ground level (AGL). A set of three microphones was used. Microphone 1 was centered on the flight path at a height of 1.2 m (4 ft). Microphone 2 was centered on the flight path at ground level. Microphones 1 and 2 are subsequently referred to as flyover microphones. Microphone 3 was perpendicular to the flight path at a distance of 10.7 m (35 ft) from microphones 1 and 2 and at ground level. Microphone 3 is subsequently referred to as the sideline microphone. Winds were calm on the day of the test. Additional details on the flight test measurements can be found in Ref. [6].

The subsequent flyover simulations will focus on one instance of the 10 m/s, 20 m AGL data. This flight test condition was closest to the tunnel test conditions and measurement locations. Figure 14(a) shows the flight speed to be rapidly accelerating on the inbound leg, mostly leveling off at around 10 seconds, then dropping rapidly after 30 s. The recorded pressure time history at flyover microphone 2 is shown in Figure 14(b). All microphone data are available for auditioning (audio samples 9-11 [12]).

V. Flyover Simulations

Acoustic wind tunnel data from simultaneous rotor (R1&R3) operations serve as the basis for the flyover simulations that follow. Flyovers were simulated according to the methods detailed in Section III. Two sets of simulations are performed. The first set of simulations is meant to verify the simulation approaches by making direct comparisons between the frequency domain method using ANOPP and the time domain method using the NAF. The second set of simulations is intended to explore what additional effects, beyond those observed in the wind tunnel data, are needed to capture the salient features of recorded flight test data. In the following, full revolution rotor data were used for the time domain simulations.

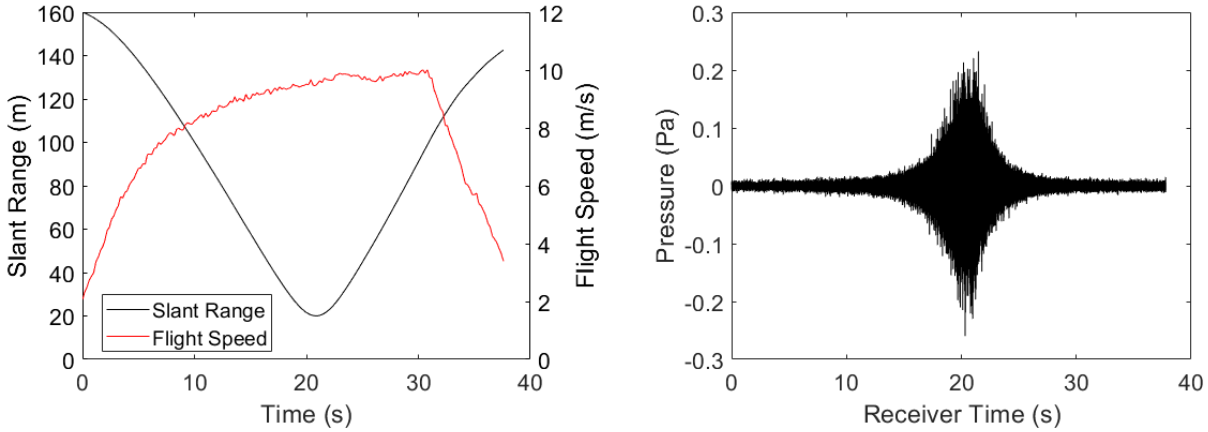

(a) Slant range and flight speed profiles. (b) Flyover microphone 2.

Figure 14: Recorded flight profiles and pressure time history of a 10 m/s, 20 m AGL flyover.

A. Verification of Simulation Methods

Data from the 45 N net thrust condition at a forward pitch angle of 10° served as the basis for this verification exercise. The flyovers were simulated at the forward flight speed corresponding to the LSAWT test condition of 15.3 m/s (50.2 ft/s). A straight and level trajectory was prescribed at an altitude of 21.8 m (71.4 ft) AGL and distance of 200 m (656 ft) on either side of the centerline observer. Two observer locations are considered; one on the ground plane along the centerline of the trajectory (subsequently referred to as the flyover observer), and one on the ground plane at a sideline distance of 10.7 m (35 ft) from the flyover observer (subsequently referred to as the sideline observer). The $\phi = 0°$ (on-axis) LSAWT data were used to simulate the flyover observer, and the $\phi = 30°$ (off-axis) data were used to simulate the sideline observer, see Figure 2(a). A hard ground plane is simulated, thus the simulated data reflect a pressure doubling at both receivers.

It is assumed that the data acquired from the simultaneous rotor (R1&R3) operations constitute half of what is expected of the entire vehicle. In order to simulate that, the data are scaled assuming incoherent summation. For the ANOPP frequency domain analysis, a gain of 3 dB was applied to the 1/3 octave band SPL data. The source was prescribed at the body center. For the NAF time domain analysis, two approaches were considered. In the first, a gain of 3 dB was applied to each separated periodic rotor component (R1 and R3), and to the broadband component. In this case, all components were colocated at the body center. In the second, the four periodic sources were separately placed at the rotor hub locations (see Ref. [1]). Waveforms for rotors R2 and R4 were replicated from those of R1 and R3, respectively, but with each having a random starting index to desynchronize. The broadband component was prescribed at the body center with a gain of 3 dB, since this component was not separable into contributions from R1 and R3.

Figure 15 provides comparisons of L_A and PNLT at the flyover observer calculated using the ANOPP and the NAF. The NAF results are provided for both colocated and spatially separated sources. The results are in excellent agreement, verifying that the approaches are equivalent insofar as their ability to generate certification metrics. Very small differences in the PNLT traces are associated with slightly different tone penalties applied to the time and frequency domain approaches. The polar emission angle θ is also shown in the lower plots. The dashed vertical lines delimit the forward and aftmost shear layer-corrected LSAWT emission angles. As previously noted, simulation at angles less than the forwardmost angle and greater than the aft-most angle is based upon the data at those angles. Therefore, the changes shown are due solely to propagation effects, namely, Doppler shift, spreading loss, and absorption. The relatively short duration highlights the need for source noise data at extended emission angles.

Integrated noise metrics L_{AE} and EPNL were computed from L_A and PNLT, respectively, using methods prescribed in Ref. [19]. The metric values are provided in Table 1 and are seen to be in excellent agreement, verifying the approaches are also equivalent on an integrated metrics basis. Simulated flyover data at the sideline observer (not shown) are also found to be in excellent agreement, as indicated by the L_{AE} and EPNL values in Table 1.

The NAF pseudorecording for the separated sources is shown in the form of a pressure time history in Figure 16(a) and a spectrogram in Figure 16(b). The leading ~0.6 seconds of zero signal reflects the propagation time from the initial position to the observer. While the waveform differs slightly between that shown in Figure 16(a) and that of the colocated sources (not shown), there is little discernable difference found upon auditioning (audio samples 12-13 [12]) or appreciable difference in the sound quality metrics derived from them (not shown). The beat frequency

between the BPF of rotors R1-R2 (135 Hz) and the BPF of rotors R3-R4 (163 Hz) is about 28 Hz, and is not apparent. The presence of shaft order frequencies between the stronger blade passage frequencies is evident in the spectrogram.

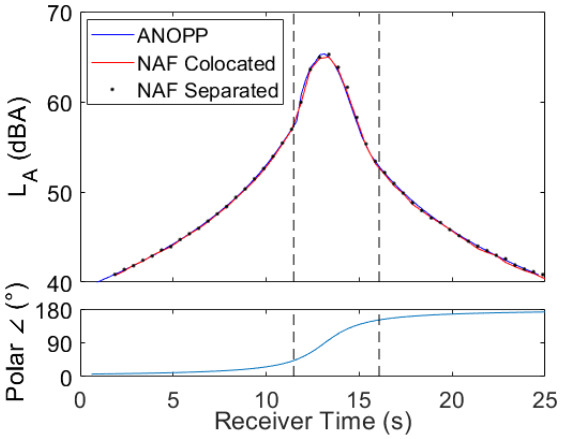

(a) Comparison of A-weighted SPL.

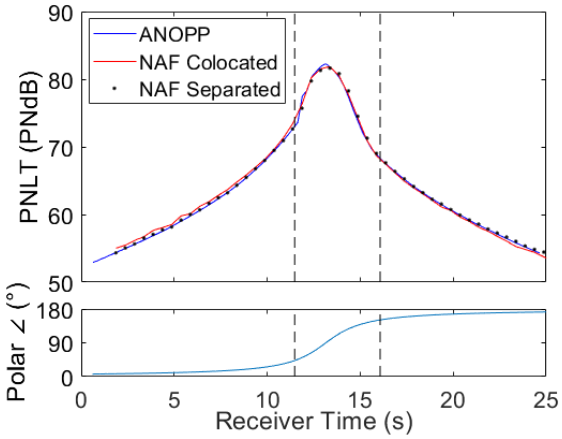

(b) Comparison of PNLT.

Figure 15: Simulated noise at the flyover observer via frequency domain (ANOPP) and time domain (NAF) approaches. Dashed vertical lines delimit bounds of LSAWT data.

Table 1: Comparison of integrated noise metrics at the flyover and sideline observers.

Observer	Metric	ANOPP	NAF Colocated	NAF Separated
Flyover	L_{AE} (dBA)	68.6	68.6	68.8
	EPNL (EPNdB)	75.2	75.3	75.2
Sideline	L_{AE} (dBA)	70.5	70.6	70.5
	EPNL (EPNdB)	77.5	77.4	77.2

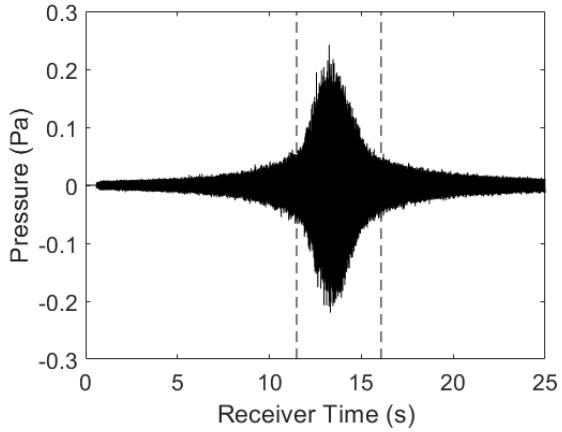

(a) Pressure time history.

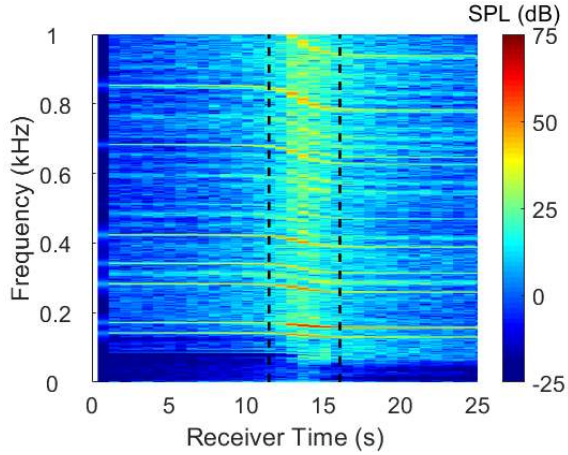

(b) Spectrogram.

Figure 16: Pressure time history and spectrogram from NAF (separated) pseudorecording at the flyover observer. Dashed vertical lines delimit bounds of LSAWT data.

B. Guided Explorations using Flight Test Data

The intention of simulating the flight test condition is to explore the need for additional modifications to the simulation process required to capture the salient features of the flight test data. In other words, the flight test data serves as a guide to identify what is missing from the simulation and is not used for validation purposes. LSAWT data from the 27 N vehicle net thrust condition at a forward pitch angle of 4° were used for this purpose. In the absence of loading data, this LSAWT data set was selected because the estimated front rotor advancing tip Mach number (0.230) was closer to the flight test condition (0.227) than any of the other LSAWT test conditions. Time domain simulations using the NAF were performed with the four rotors components separated and broadband component at

the body center. Frequency domain simulations using the ANOPP were performed with the single source at the body center.

Because the LSAWT data were acquired at a free stream Mach number of 0.046 (15.6 m/s) and are compared with flight test data at a forward flight speed of roughly 9.5 m/s, some adjustments to the wind tunnel data are needed to compensate for simulating the flight test condition. The difference in the ground track speed affects the duration and consequently the integrated metrics L_{AE} and EPNL. This can readily be compensated by specifying a simulation flight speed equal to that of the flight test, specifically, that indicated in Figure 14(a). The trajectory was specified as straight and level, at an altitude of 20.03 m (65.7 ft) AGL, corresponding to the point of closest passage over microphone 2. Given that the wind tunnel data do not precisely match the flight test condition, the comparisons of L_A and PNLT are remarkably good within the limits of the LSAWT data, as seen in Figure 17 for the flyover observer (microphone 2) location. Similar quality comparisons (not shown) are found at the sideline observer (microphone 3) location. Of course, differences exist because the loading conditions differ by some unknown amount. However, in the absence of such data, the quality of the comparisons demonstrates the effectiveness of matching ground and flight test conditions on the basis of advancing tip Mach number. Integrated metrics also compare very well, as indicated in Table 2, since the duration of the data needed for those calculations lie mostly within the limits of the LSAWT data. As an aside, it is interesting to note that the metrics are higher for the flyover observer than the sideline observer, in contrast to the opposite trend at the higher loading condition at 10° forward pitch angle (see Figure 15 and Table 1), indicating a source directivity dependency on loading condition and pitch angle.

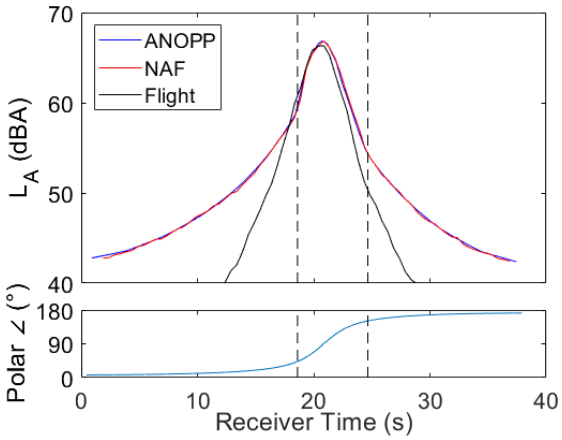

(a) Comparison of A-weighted SPL.

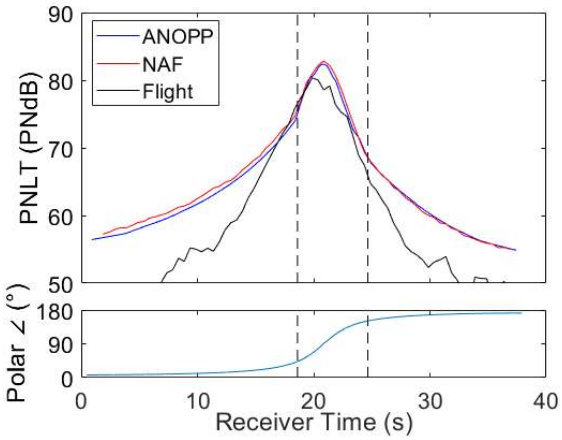

(b) Comparison of PNLT.

Figure 17: Comparison of metrics from simulations and flight test data at flyover observer (microphone 2). Dashed vertical lines delimit bounds of LSAWT data.

Table 2: Comparison of integrated noise metrics at the flyover and sideline observers.

Observer	Metric	ANOPP	NAF Separated	Flight
Flyover (Mic. 2)	L_{AE} (dBA)	71.6	71.6	71.1
	EPNL (EPNdB)	76.8	77.4	75.4
Sideline (Mic. 3)	L_{AE} (dBA)	69.5	69.5	68.7
	EPNL (EPNdB)	74.8	74.6	73.9

For the time domain simulation, differences in the blade passage frequency in excess of the pure tone just noticeable difference (JND) in frequency of 1 Hz [15] will be apparent when auditioning the flight test recording and the simulation pseudorecording. Therefore, it is of interest to tune the BPF of the simulation to that of the flight test. In the absence of an onboard sensor to measure rotor RPM, the spectrogram may be used for this purpose. Figure 18(a) shows the spectrogram of the microphone 2 recording. Note the presence of a significant low frequency background noise below about 150 Hz for the duration of the recording. The Doppler shift is most noticeable about the overhead position at 20.8 seconds. Figure 18(b) provides a close-up in that timeframe. It is seen that the forward pair of rotors (R1 and R2) have BPFs of about 113 and 117 Hz, while the aft pair (R3 and R4) have BPFs of about 141 and 145 Hz. Similar differences in BPFs were observed in other quadcopter flight test and simulated recordings, and the effects were found to be audible [20]. It is not possible to tell from the data which rotor is operating at which RPM, other than the fore/aft difference. This difference in RPM also gives rise to beating at the difference frequency of about

4 Hz, the effects of which are visible in Figure 18(a) as a modulation in spectral amplitude. A frequency offset (tuning) can be added to the simulation by simply expanding or contracting the timebase of the periodic signal. This operation is performed to tune the BPF of forward rotors R1 and R2 from the LSAWT test BPF of roughly 105 Hz to 113 and 117 Hz, respectively. Similarly, the BPF of aft rotors R3 and R4 are tuned from the LSAWT test BPF of roughly 128 Hz to 141 and 145 Hz, respectively. In conjunction with that operation, the starting index of the waveform is varied between rotors R1 and R2, and between rotors R3 and R4. Note that no measures are taken to shift the frequency vector of the broadband noise component, because there is no evidence, e.g., a broadband JND in frequency, to suggest the result would be audible. In the absence of flight test data to guide this tuning, flight dynamics models can be used to determine both steady and unsteady RPM distributions in flight [20].

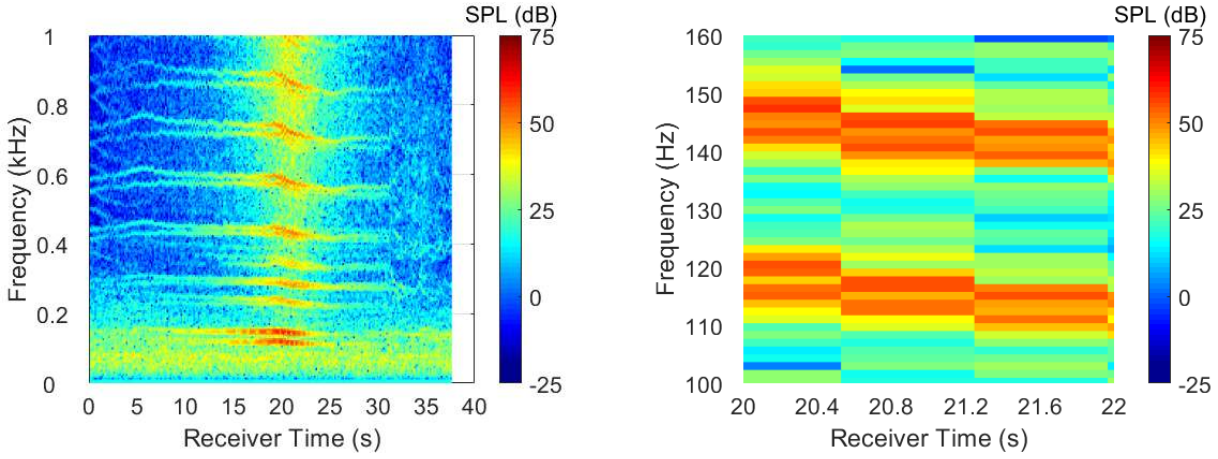

(a) Full flyover. (b) Close-up at overhead position.

Figure 18: Spectrograms of microphone 2 recording in SPL (dB), see Figure 14(b).

The RPM tuning has negligible effect on L_A (not shown), increasing L_{AE} from 71.6 to 71.7 dBA at the flyover observer, and from 69.5 to 69.6 dBA at the sideline observer. A minor effect on PNLT (not shown) is noted, decreasing EPNL from 77.4 to 76.4 EPNdB at the flyover observer, and from 74.6 to 73.6 EPNdB at the sideline observer. In contrast, audible differences between the two sets of pseudorecordings (audio samples 14-15 [12]), i.e., at the untuned LSAWT BPFs and at the tuned flight BPFs, are readily apparent in two ways. First, by tuning the LSAWT BPFs to flight conditions, the perceived differences between the tuned pseudorecordings and microphone recordings are reduced (interleaved audio samples 16-17 [12]). Further, beating is audible in the tuned pseudorecording, and not in the untuned pseudorecording, and the effect is visible in the spectrograms shown in Figure 19. The lack of low frequency background noise in the pseudorecordings is apparent when comparing Figure 19 to Figure 18(a) and upon auditioning.

The difference in roughness observed between the wind tunnel and synthesized source noise remains apparent in the propagated noise. Figure 20 shows the wavelet energy spectra of the microphone 2 recording and of the tuned NAF pseudorecording at the overhead position. The amplitude modulation of the high frequency broadband noise is apparent in the former, indicating that it is not particular to the LSAWT test data. It is not apparent in the tuned or untuned (not shown) NAF pseudorecordings. This characteristic is also indicated as a large difference in roughness (not shown).

The same BPF tuning is used to simulate the noise at the 1.2 m flyover observer (microphone 1). The Delany-Bazley 1-parameter impedance model [21] is used, with the flow resistivity taken as 150,000 Pa s/m^2 for grass. This selection was based solely on a test site photograph. The integrated metrics L_{AE} and EPNL compare reasonably well, with NAF simulated values 67.3 dBA and 71.1 EPNdB, respectively, compared to flight recording values of 67.8 dBA and 73.7 EPNdB, respectively. Spectrograms, shown in Figure 21, show similar interference patterns due to the superposition of direct and ground reflected waves, with the pattern accentuated by greater broadband content in the NAF simulation. The ground plane reflection displays a distinct effect upon auditioning (audio samples 18-19 [12]).

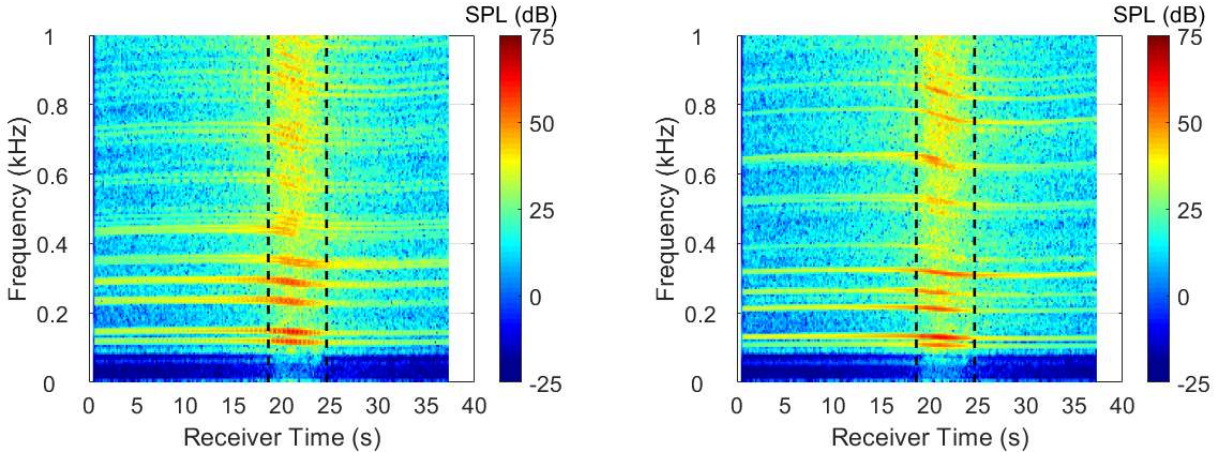

(a) Tuned. (b) Untuned.

Figure 19: Spectrograms of BPF tuned and untuned pseudorecordings. Dashed vertical lines delimit bounds of LSAWT data.

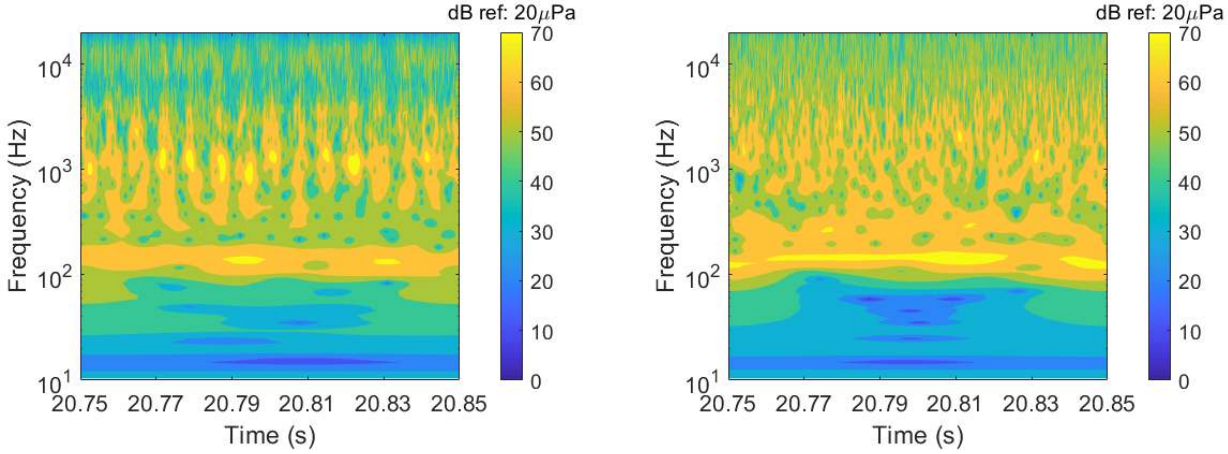

(a) Microphone 2 recording. (b) Tuned NAF pseudorecording.

Figure 20: Wavelet energy spectra of microphone 2 and tuned NAF pseudorecording.

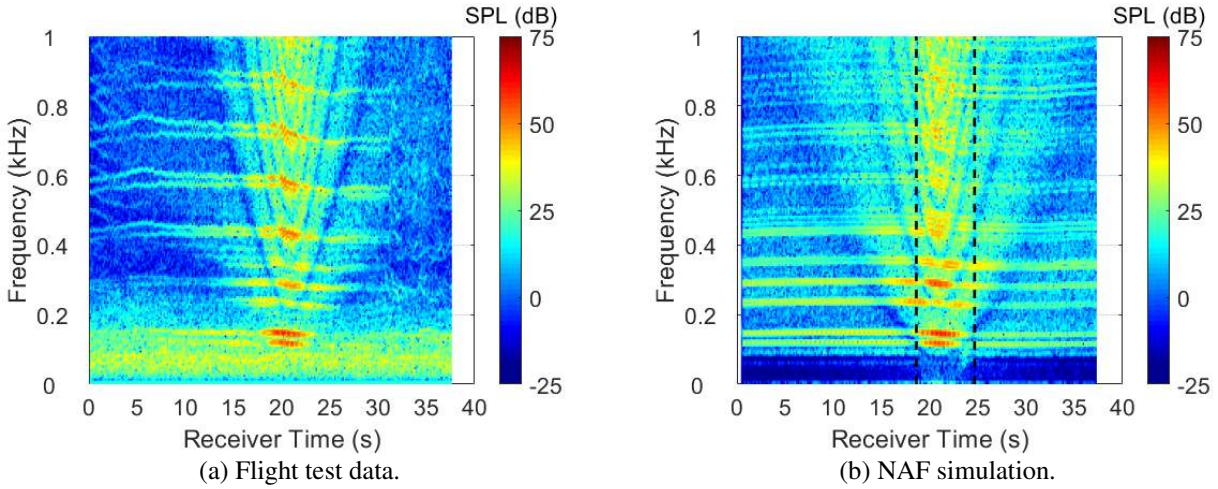

(a) Flight test data. (b) NAF simulation.

Figure 21: Spectrograms from flight test data and NAF simulation at flyover observer (microphone 1). Dashed vertical lines delimit bounds of LSAWT data.

VI. Conclusions

A study was performed to assess the effectiveness of using acoustic wind tunnel data of a small unmanned aerial system for the simulation of its flyover noise. Two methods were offered for doing so: a frequency domain approach using the NASA Aircraft NOise Prediction Program and a time domain approach using the NASA Auralization Framework. Both methods utilized the same underlying acoustic wind tunnel data as their basis, but employed method-dependent data processing. The methods were verified to provide consistent simulated flyover results at receiver locations on the ground.

Over the course of the study, comparisons of time domain simulation results with both wind tunnel and flight test data led to observations important to human perception, namely,

- The simulation of shaft order harmonics using one full revolution of data more closely mimics the recorded sound, even though a single time-averaged blade passage produces nearly the same waveform and sound pressure level.
- Amplitude fluctuations of high frequency broadband noise at the blade passage frequency significantly affect the character of the signal, giving it increased roughness. This feature was observed in both wind tunnel and flight test data, and was absent in the simulations using the present methods.
- Tuning of BPFs to flight conditions allows time domain simulations to capture the beating between closely spaced rotor RPMs.

Additionally, the following general observations were made:

- A greater range of emission angle data in both the forward and aft directions would be of value. As it stands, the LSAWT linear array is marginally capable of measuring data needed for calculating L_{AE} and EPNL of low flying sUAS.
- Matching advancing tip Mach number of wind tunnel data with the desired flight condition was shown to be a useful strategy in the absence of loading data.
    - In conjunction with the above, a change of flight speed from tunnel to the desired flight condition was shown to be perceptually important as it affects the duration of the event, and consequently the values of L_{AE} and EPNL.

Several developments going forward would help increase the fidelity of the simulations. First, current methods for experimentally and analytically/numerically determining time-averaged broadband noise are insufficient for simulating the roughness character. Analysis tools need to be enhanced to quantify the effect, and sound synthesis tools need to be able to incorporate that effect. Likewise, given the unsteady flight of sUAS, further development of flight dynamics models would aid in quantifying RPM distributions on multipropeller/multirotor vehicles. Additional developments of NAF source noise synthesis methods are needed to take advantage of time varying RPMs. It is expected that these developments and the lessons learned in this study will be applicable to larger, passenger carrying urban air mobility vehicles.

Acknowledgments

The authors wish to acknowledge Aric Aumann, Science Applications International Corporation, for development of the NAF narrowband synthesis advanced plugin library used in this work, and Andy Christian, NASA Langley Structural Acoustics Branch, for helpful discussions related to fluctuations of high frequency broadband noise. The authors would also like to give a special thanks to John Swartzbaugh, Stanley Mason, Jeffrey Collins and Bryan Lamb of the NASA Langley LSAWT, for their efforts in facility test setup and data acquisition. This work was funded by the NASA Convergent Aeronautics Systems (CAS) and Transformational Tools and Technologies (TTT) projects of the Transformative Aeronautics Concepts Program (TACP), and by the NASA Revolutionary Vertical Lift Technology (RVLT) project of the Advanced Air Vehicles Program (AAVP).

References

[1] Zawodny, N.S. and Pettingill, N.A., "Acoustic wind tunnel measurements of a quadcopter in hover and forward flight conditions," *InterNoise 2018*, Paper 1364, Chicago, IL, August 26-29, 2018.

[2] Zawodny, N.S. and Haskin, H., "Small propeller and rotor testing capabilities of the NASA Langley Low Speed Aeroacoustic Wind Tunnel," *23rd AIAA/CEAS Aeroacoustics Conference*, AIAA-2017-3709, Denver, CO, 2017.
[3] Zorumski, W.E., "Aircraft noise prediction program theoretical manual," NASA TM-83199, 1982.
[4] Aumann, A.R., Tuttle, B.C., Chapin, W.L., and Rizzi, S.A., "The NASA Auralization Framework and plugin architecture," *InterNoise 2015*, San Francisco, CA, August 9-12, 2015.
[5] Rizzi, S.A. and Sahai, A.K., "Auralization of air vehicle noise for community noise assessment," *CEAS Aeronautical Journal*, Vol. 10, No. 1, pp. 313-334, 2019.
[6] Christian, A. and Cabell, R., "Initial investigation into the psychoacoustic properties of small unmanned aerial system noise," *23rd AIAA/CEAS Aeroacoustics Conference*, AIAA-2017-4051, Denver, CO, 2017.
[7] Rizzi, S.A., Stephens, D.B., Berton, J.J., Van Zante, D.E., Wojno, J.P., and Goerig, T.W., "Auralization of flyover noise from open rotor engines using model scale test data," *AIAA Journal of Aircraft*, Vol. 53, No. 1, pp. 117-128, 2016.
[8] Amiet, R.K., "Refraction of sound by a shear layer," *Journal of Sound and Vibration*, Vol. 58, No. 4, pp. 467-482, 1978.
[9] Pera, N.M., Rizzi, S.A., Krishnamurthy, S., Fuller, C.R., and Christian, A.W., "Development of a method for analysis and incorporation of rotorcraft fluctuation in synthesized flyover noise," *AIAA SciTech 2018*, AIAA-2018-0267, Kissimmee, FL, 2018.
[10] Lopes, L.V. and Burley, C.L., "ANOPP2 User's Manual: Version 1.2," NASA TM-2016-219342, 2016.
[11] Krishnamurthy, S., Rizzi, S.A., Boyd Jr., D.D., and Aumann, A.R., "Auralization of rotorcraft periodic flyover noise from design predictions," *74th AHS Forum*, Paper 166, Phoenix, AZ, 2018.
[12] "Aircraft flyover simulation," https://stabserv.larc.nasa.gov/flyover/, NASA, 2019.
[13] Christian, A., Caston, J., and Greenwood, E., "Regarding the perceptual significance and characterization of broadband components of helicopter source noise," *Forum 75, Vertical Flight Society*, Paper 83, Philadelphia, PA, 2019.
[14] Stephenson, J.H. and Tinney, C.E., "Extracting blade-vortex interactions using continuous wavelet transforms," *Journal of the American Helicopter Society*, Vol. 62, No. 2, pp. 1-10, 2017.
[15] Zwicker, E. and Fastl, H., *Psychoacoustics, Facts and Models*, Third ed. Berlin, Springer-Verlag, 2006.
[16] Daniel, P. and Weber, R., "Psychoacoustical roughness: Implementation of an optimized model," *Acta Acustica united with Acustica*, Vol. 83, No. 1, pp. 113-123, 1997.
[17] "ISO 532-1:2017, Acoustics - Methods for calculating loudness - Part 1: Zwicker method," 2017, pp. 58.
[18] "Measurement technique for the simulation of the auditory sensation of sharpness," Deutsches Institut für Normung (DIN) 45692, 2009.
[19] "Annex 16 to the Convention on International Civil Aviation, Environmental Protection, Volume I, Aircraft Noise (7th Edition)," International Civil Aviation Organization, Montreal, Canada, 2014, pp. 236.
[20] Christian, A.W. and Lawrence, J., "Initial development of a quadcopter simulation environment for auralization," *72nd AHS Forum*, West Palm Beach, FL, 2016.
[21] Delany, M.E. and Bazley, E.N., "Acoustical properties of fibrous absorbent materials," *Applied Acoustics*, Vol. 3, No. 2, pp. 105-116, 1970.